Survey Review

ISSN: 0039-6265 (Print) 1752-2706 (Online) Journal homepage: http://www.tandfonline.com/loi/ysre20

An adaptive stochastic model for GPS observations and its performance in precise point positioning

J. Z. Zheng & F. Guo

To cite this article: J. Z. Zheng & F. Guo (2016) An adaptive stochastic model for GPS observations and its performance in precise point positioning, Survey Review, 48:349, 296-302, DOI: 10.1179/1752270615Y.0000000033

To link to this article: https://doi.org/10.1179/1752270615Y.0000000033

Published online: 30 Mar 2016.

Submit your article to this journal

Article views: 94

View Crossmark data

Full Terms & Conditions of access and use can be found at
http://www.tandfonline.com/action/journalInformation?journalCode=ysre20

An adaptive stochastic model for GPS observations and its performance in precise point positioning

J. Z. Zheng[1] and F. Guo*[2]

In this paper, the stochastic characteristics of Global Positioning System (GPS) pseudo-range noise as influenced by several factors such as receiver type, frequency, and ionosphere environment are analysed. The results indicate that the noise level of GPS observations is significantly affected by these factors. Moreover, the noise level is so mutable that it cannot be generalised and described by a uniform empirical model. Even for the same satellite, the noise level of observations may fluctuate sharply in both spatial and temporal resolution. To establish a reasonable stochastic model, a recursive sliding window method for estimating pseudo-range noise in real time is introduced. The effectiveness of the proposed method is verified by specific computational examples.

Keywords: GPS, Multipath effect, Stochastic model, Pseudo-range noise, Real-time estimation

Introduction

It is important to construct both accurate functional and stochastic models so that reliable GPS positioning solutions can be developed. A functional model describes the functional relationship between the observations and the parameters to be estimated, whereas a stochastic model reflects statistical characteristics, which cannot be fully represented by the functional model. This paper discusses stochastic models of GPS observations, in particular, how to determine the prior variance–covariance matrix. Among the popular stochastic models are the satellite elevation method, the signal-to-noise ratio method, the least-squares residual error method, and real-time estimation approaches (Wang *et al.*, 2002; Satirapod and Luansang, 2008). The residual error-based statistical method depends on the reliability of the prior variance matrix. If the prior variance matrix is not reasonably accurate, the residual errors will be redistributed after adjustment. Hence, this method may distort the statistical information in GPS observations (He, 2002). Both the GPS satellite elevation functional method and the signal-to-noise functional method are simple and easy to implement, but the coefficients involved in these two methods are determined based on an empirical model and therefore cannot reflect the actual noise level of the GPS observations. For instance, when the GPS satellite elevation or the signal-to-noise ratio is large, the variance of the pseudo-range and phase observations can be directly fixed to given values, e.g. 0.3 and 0.003 m, respectively. The variance ratio between the pseudo-range and phase observations can also be fixed to given values for stochastic models (Satirapod and Luansang, 2008; Tiberius and Kenselaar, 2000). However, such empirical stochastic models cannot describe the statistical characteristics of GPS observations under all conditions. As a result, they will degrade the obtainable positioning accuracy.

The stochastic noise in GPS observations includes measurement noise and multipath effects. Stochastic noise is related to many factors such as the type of receiver, the type of observations, the satellite elevation, the measurement model, and the specific measurement environment. Because these factors vary significantly during the measurement process, it is impossible to determine a universal prior variance–covariance matrix in advance. To determine an appropriate stochastic model for GPS observations, a first step is to analyse the relationship between the stochastic characteristics of pseudo-range noise and the factors, which may influence observation accuracy. Then an adaptive stochastic model will be proposed to estimate pseudo-range noise in real time. This model uses a fixed sliding window to estimate the noise in GPS pseudo-range observations. In addition, attenuation factors will be introduced to decrease the contribution of old information and to take account of temporal variations in pseudo-range noise. This will result in a stochastic model, which can dynamically reflect time-varying noise in pseudo-range observations. Finally, the effectiveness of the proposed method will be verified numerically using field datasets.

Analysis of the stochastic characteristics of observation noise

A few case studies are performed to demonstrate that the pseudo-range noises (and multipath) vary with receiver types, frequency and observing environment in this section.

[1]College of Civil Engineering, Nanjing Forestry University, 159 Lonpan Road, Nanjing 210037, China
[2]School of Geodesy and Geomatics, Wuhan University, 129 Luoyu Road, Wuhan 430079, China

*Corresponding author, email fguo@whu.edu.cn

© 2016 Survey Review Ltd
Received 29 January 2015; accepted 14 April 2015
DOI 10.1179/1752270615Y.0000000033

Pseudo-range noise of different types of receivers

Pseudo-range noise was investigated by a flight test [Universal Time Coordinate (UTC) 10–16, 5 August 2005]. Four different types of receivers were set up on the same plane (TRIMBLE4000SSI, ASHTECH UZ-12, TPS LEGACY, and TPS EGGDT), hereafter referred to as RCV1, RCV2, RCV3, and RCV4, respectively. These receivers were arranged close to each other, with the longest baseline length being only about 3 m. Hence, it could be assumed that the observation environment and measurement mode of these receivers were the same. The TEQC software (Estey and Meertens, 1999) was used to calculate the multipath effects of the pseudo-range noise (P1). Taking P1 as an example, Fig. 1 shows the pseudo-range noise of the four types of receiver.

Figure 1 shows that the pseudo-range noise is related to the satellite elevation of the GPS observations. When the satellite elevation is $<20°$, its noise curve can be approximated by a sine or cosine function; when the satellite elevation angle is greater than 20°, the correlation between satellite elevation and noise level is so weak that the noise level can be represented as a constant. However, the characteristics of pseudo-range noise are significantly different for different types of receivers, especially between RCV2 and RCV4. The root mean square (RMS) errors of pseudo-range noise for the four types of receivers were 0.335, 0.731, 0.348, and 0.265 m, respectively. Apparently, if the variance of pseudo-range observation noise is simply fixed to $(0.3\ \text{m})^2$ or some other given value, the variance of some observations will be larger than the true variance, whereas that of others will be smaller. The stochastic model used therefore fails to reflect properly the actual distribution of pseudo-range noise.

Pseudo-range noise at different frequencies

Traditional stochastic models for GPS observations assume no difference in noise generated at different frequencies, or in other words, the noise levels of GPS observations at different frequencies are assumed to be constant. Considering that the accuracy of phase observations is higher than that of pseudo-range observations by two or three orders of magnitude and that the accuracy variation in phase observation noise at different frequencies is small, only the stochastic characteristics of pseudo-range noise at different frequencies are discussed in this section.

Static observations recorded at the International GNSS Service (IGS) NKLG tracing station on April 17 2004 were used for the analysis performed in this research (the receiver type was TRIMBLE 4000SSI). The TEQC software was first used to calculate the pseudo-range noise for all satellites at frequencies L1 and L2. The corresponding results were recorded as MP1 and MP2 and arranged in time sequences, as shown in Figs. 2 and 3. In these two figures, the horizontal axis represents the UTC, and the vertical axis represents the satellite number. The distance between two adjacent scale markers represents 1 m. Similarly, the relationship between satellite elevation and pseudo-range noise is shown in Fig. 4.

From Figs. 3 and 4, it is apparent that all the MP2 were significantly larger than the MP1, indicating that

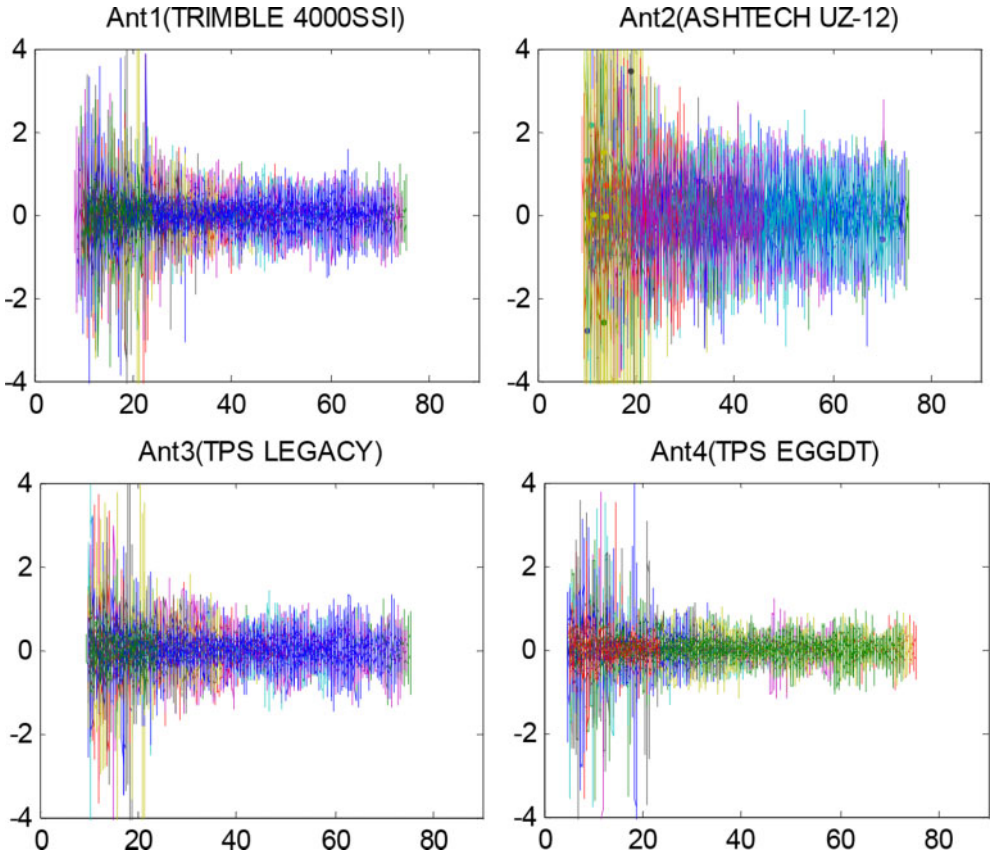

1 Pseudo-range (P1) noise of four types of receiver. For each plot, the horizontal axis represents the satellite elevation angle (units: degrees), and the vertical axis represents the corresponding noise (units: metre)

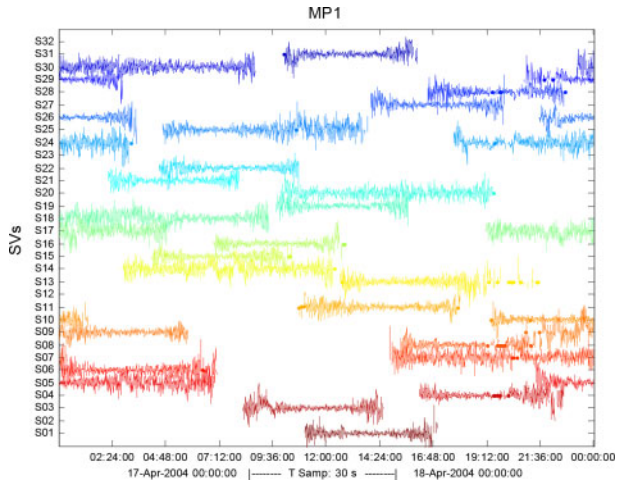

2 Time series of pseudo-range (P1) noise of all satellites at NKLG

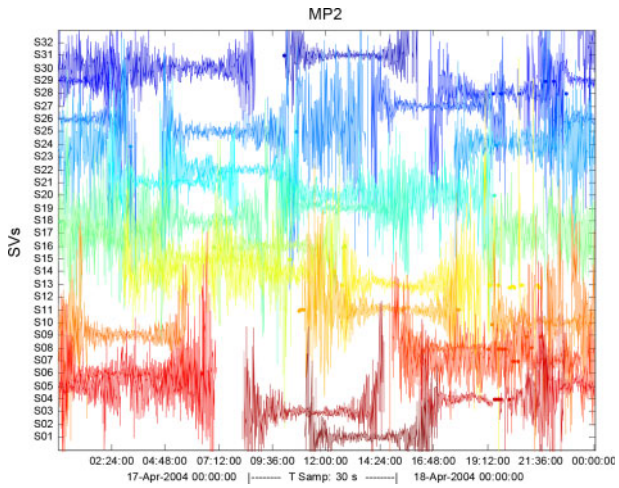

3 Time series of pseudo-range (P2) noise of all satellites at NKLG

the observation noise in P2 was obviously greater than that in P1, especially when the satellite dropped to a low elevation. Unlike the computational examples in Pseudo-range noise of different types of receivers Section, the pseudo-range noise in this example was highly correlated with satellite elevation, meaning that its noise curve can be represented by a sine or cosine function over the entire arc. The calculated RMS errors of MP1 and MP2 were 0.367 and 1.622 m, respectively.

Obviously, these results indicate that the assumption that observations have the same accuracy at different frequencies is not realistic. This is particularly true for the cross-correlation type of receiver because anti-spoofing generally makes the observation accuracy at frequency L2 lower than at L1.

Pseudo-range noise under other abnormal conditions

The accuracy of GPS observations can be affected by other factors. Figure 5 presents the distribution of pseudo-range noise arranged by satellite elevation for frequencies L1 and L2. The data were acquired at IGS stations ALIC and ALGO on day of year (doy) 46 in 2010. To highlight the abnormality of the pseudo-range noise even at high satellite elevation, only satellite elevations from 30° to 90° are shown.

As shown in Fig. 5, the P1 observation noise of satellite G01 at ALIC station was obviously greater than that of the other satellites, and the value of MP1 remained large even when the satellite elevation was $>60°$. Meanwhile, at the ALGO station, the MP2 for several GPS satellites (such as G03, G18, and G21) became clearly abnormal, with various spikes randomly appearing during both rising and declining periods. Because the observation abnormalities corresponded to different satellites at the two stations, the possibility of problems with the satellites can be excluded. Further analysis revealed that the time-series pattern of the pseudo-range noise at these two stations was similar to that shown in Fig. 5. Work conducted by the Geoscience Australia attributes the decline in the data quality at the ALIC station to the aging and erosion of the hardware in the receiver stations (IGSSTATION-3728, 2010). Although Natural Resources Canada (NRC) has not provided an explanation for the decline in data quality for the stations, they assumed that this phenomenon was perhaps linked to the receiver channel because the abnormality occurred only on certain satellites (IGSSTATION-3860, 2010).

High-voltage radiation and electromagnetic interference (EMI) can also contribute to accuracy decline in GPS observations. For instance, ionosphere scintillation can affect pseudo-range noise, as shown in Figs. 6 and 7. The horizontal axis represents UTC; the vertical axis

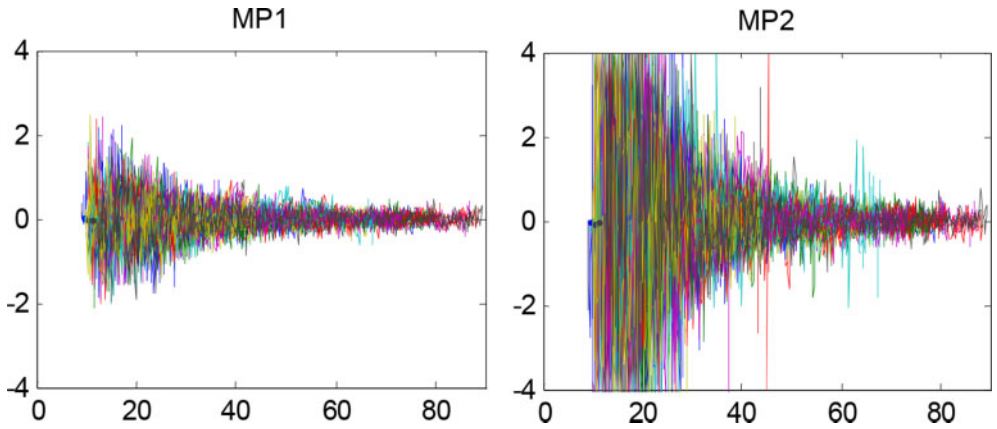

4 Comparison of pseudo-range noise at different frequencies (NKLG station). For each plot, the horizontal axis represents the satellite elevation (units: degrees), and the vertical axis represents the corresponding noise (units: metre)

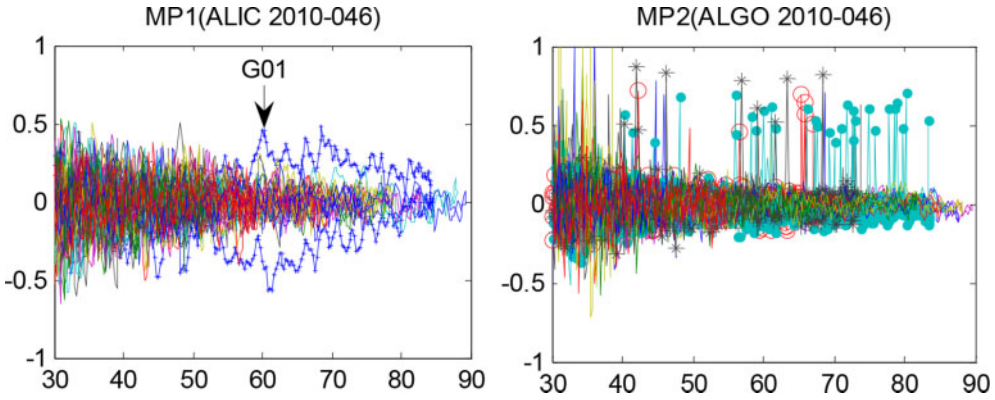

5 Relation between satellite elevation angle and pseudo-range noise at the ALIC and ALGO stations. For each plot, the horizontal axis represents the satellite elevation angle (units: degrees), and the vertical axis represents the corresponding noise (units: metre)

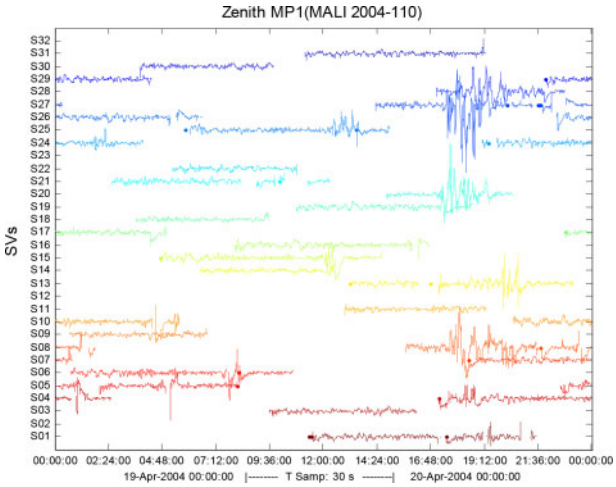

6 Time series of pseudo-range (P1) noise for all satellites in the zenith direction at the MALI station

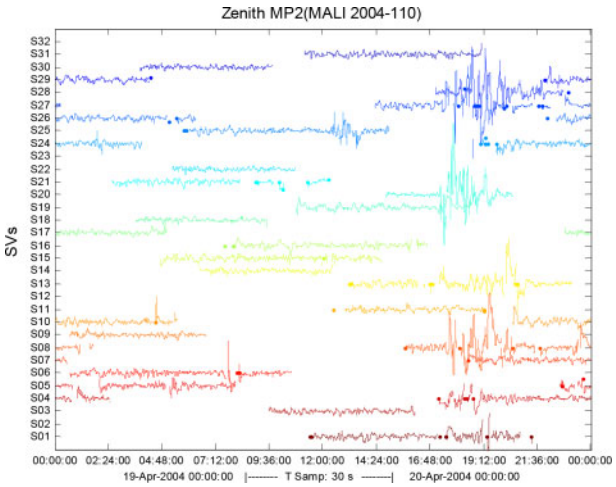

7 Time series of pseudo-range (P2) noise for all satellites in the zenith direction at the MALI station

represents pseudo-range noise with pseudo-random noise (PRN) for all satellites. The distance between two adjacent scale markers represents 1 m. To eliminate the influence caused by satellite elevation, MP1 and MP2 were projected to the zenith direction using a sine or cosine function. In this way, pseudo-range noise for all satellites in the zenith direction could be obtained.

Figures 6 and 7 show that using a sine or cosine function can capture the stochastic characteristics of pseudo-range noise as a function of satellite elevation during the quiet period of the ionosphere (before UTC 17:00:00), and that afterwards the noise obtained from the zenith direction basically reflects the real level of pseudo-range noise. Noise levels for all satellites were consistent overall as well. However, when ionosphere scintillations were present (UTC 17:00:00–22:00:00), the variance among the pseudo-range noise from different satellites was large. If the pseudo-range noise of satellites, which pass through the ionosphere's scintillating part, was fluctuating markedly, such as for G08, G13, G20, G27, and G28, their MP1 and MP2 were far larger than during the quiet period, whereas the pseudo-range noise of other satellites remained the same during both quiet and scintillation periods in the ionosphere.

In summary, observation noise varies with a number of factors, such as receiver type, frequency, and environment. Observation noise should therefore be carefully modelled rather than given simple empirical values.

Real-time estimation method for pseudo-range noise

This section first describes the development of an adaptive stochastic model. Afterwards, positioning tests conducted to verify the effectiveness of the proposed method are outlined.

Basic models

A linear combination that can be used to determine the code noise is the so-called code-minus-phase (De Bakker *et al.*, 2012; De Bakker *et al.*, 2009).

$$P_1 - L_1 = 2I_1 - \lambda_1 N_1 + M_1 - m_1 \quad (1)$$

$$P_2 - L_2 = 2I_2 - \lambda_2 N_2 + M_2 - m_2 \quad (2)$$

where P_i and L_i represent the GPS pseudo-range observation and phase observation at frequency i ($i = 1, 2$), respectively; I_i is the ionospheric delay; λ represents the wavelength of the carrier phase; N represents carrier-phase ambiguity; and M and m represent pseudo-range observation noise and phase

observation noise, respectively, including observation noise and multipath effects.

Since the ionospheric delay at the second frequency can be expressed as

$$I_2 = \alpha I_1, \alpha = \frac{f_1^2}{f_2^2} \tag{3}$$

Substituting equation (3) into equations (1) and (2) yields

$$M_1 = P_1 - \left(1 + \frac{2}{\alpha - 1}\right) L_1 + \frac{2}{\alpha - 1} L_2 + B_1 \tag{4}$$

$$M_2 = P_2 - \frac{2\alpha}{\alpha - 1} L_1 + \left(\frac{2\alpha}{\alpha - 1} - 1\right) L_2 + B_2 \tag{5}$$

where

$$B_1 = \left(1 + \frac{2}{\alpha - 1}\right)\lambda_1 N_1 - \frac{2}{\alpha - 1}\lambda_2 N_2 + \left(1 + \frac{2}{\alpha - 1}\right) m_1 - \frac{2}{\alpha - 1} m_2 \tag{6}$$

$$B_2 = \frac{2\alpha}{\alpha - 1}\lambda_1 N_1 - \left(\frac{2\alpha}{\alpha - 1} - 1\right)\lambda_2 N_2 + \frac{2\alpha}{\alpha - 1} m_1 - \left(\frac{2\alpha}{\alpha - 1} - 1\right) m_2 \tag{7}$$

Assuming no observable cycle slip on the carrier phase, and ignoring the observation noise of the carrier phases, B1 and B2 can be regarded as constants. Therefore, M1 and M2 will also fluctuate around constants. A sliding window method is used here to estimate the level of pseudo-range noise in real time based on the time sequence of M1 and M2.

Assuming that the size of the sliding window is n (epoch number), the first step is to carry out some pre-processing on the M sequence by subtracting the mean value

$$M'_1 = M_1 - < M_1 > \tag{8}$$

$$M'_2 = M_2 - < M_2 > \tag{9}$$

where $< M1 >$ and $< M2 >$ are, respectively, the mean value of M1 and M2 over a certain continuous arc. The pseudo-range noise (MP1 and MP2) calculated earlier using TEQC is actually M'_1 and M'_2 as defined in equations (8) and (9).

On this basis, statistical analysis can be performed on the M' sequence to obtain the pseudo-range variance at the current epoch

$$\mathrm{D}(M')_i = \frac{1}{n-1}\sum_{k=0}^{n-1} (M'_{i-k})^2 \tag{10}$$

Note that the pseudo-range noise obtained from equations (8) and (9) includes multipath effects, which have periodicity. When the size of the sliding window n is small, the pseudo-range variance obtained from Eq. (10) varies significantly and has difficulty reflecting the periodic influence caused by multipath effects. One solution is to increase the size of the sliding window, but this can decrease the tracking sensitivity for pseudo-range accuracy. To reflect the periodic characteristics of multipath effects while maintaining sensitive tracking of the time-varying characteristics of pseudo-range noise, the size of the sliding window should be fixed in a range of 5–10 min, and the 'fading memory' approach should be used to replace the variance of pseudo-range observations obtained in equation (10)

$$\mathrm{D}(M')_i = \sum_{k=0}^{n-1} \beta_k (M'_{i-k})^2 \Big/ \sum_{k=0}^{n-1} \beta_k \tag{11}$$

where β ($0 < \beta \leq 1$) is a fading factor, which can be calculated by the following formula

$$\beta_k = \frac{9}{k+9}, 0 \leq k \leq n-1 \tag{12}$$

Obviously, introduction of the fading factor will reduce the contribution of earlier information when calculating the instantaneous variance, which will then affect the ability of the stochastic model to reflect the dynamic impact of pseudo-range noise variations.

Positioning performance and discussion

To verify the effectiveness of the proposed method, precise point positioning (PPP) was performed with two different schemes using the same data as in Analysis of the stochastic characteristics of observation noise Section (for NKLG and ALIC).

In Scheme 1, the pseudo-range noise was assumed to be the same at both frequencies. The unit weight mean error was fixed as 0.3 m. Then the observation stochastic model weighted by satellite elevation was used to determine the variance matrix of the pseudo-range observations. Finally, the fixed pseudo-range to phase ratio (100 : 1) was used to determine the variance matrix of the phase observations.

In Scheme 2, the adaptive stochastic model was used to determine the variance matrix of the dual-frequency pseudo-range observations; the variance of the carrier-phase observations was determined in the same way as in Scheme 1.

The ionosphere-free carrier phase as well as pseudo-range observations were simultaneously processed (Kouba and Héroux, 2001). The elevation cutoff angle was set to 10°. Precise GPS satellite ephemeris and clock products provided by IGS were used to remove the satellite orbit and clock errors (Dow *et al.*, 2009). Tropospheric delays of the dry component were corrected by Saastamonien model, while the zenith wet tropospheric delays were estimated as random walk process. Receiver coordinates as well as receiver clock biases were modelled as white noise process in kinematic PPP, while the carrier-phase ambiguities were assumed to be constants in a continuous arc if no cycle slip occurs. The positioning results were compared with the IGS weekly published coordinates. In general, the reference coordinates have an accuracy of few millimetres.

Figure 8 shows the positioning results at the NKLG station using the two schemes during UTC 0:00–18:00. E1, N1, and U1 represent the positioning bias in the East, north, and vertical directions in Scheme 1; E2, N2, and U2 represent these biases in Scheme 2.

The positioning bias at the NKLG station shown in Fig. 8 indicates that the positioning accuracy of Scheme 1 was worse than that of Scheme 2, with a longer convergence time. This is particularly pronounced for the first few hours in the upward direction. Moreover, an obvious fluctuation of the positioning bias in the Eastward direction could be observed during

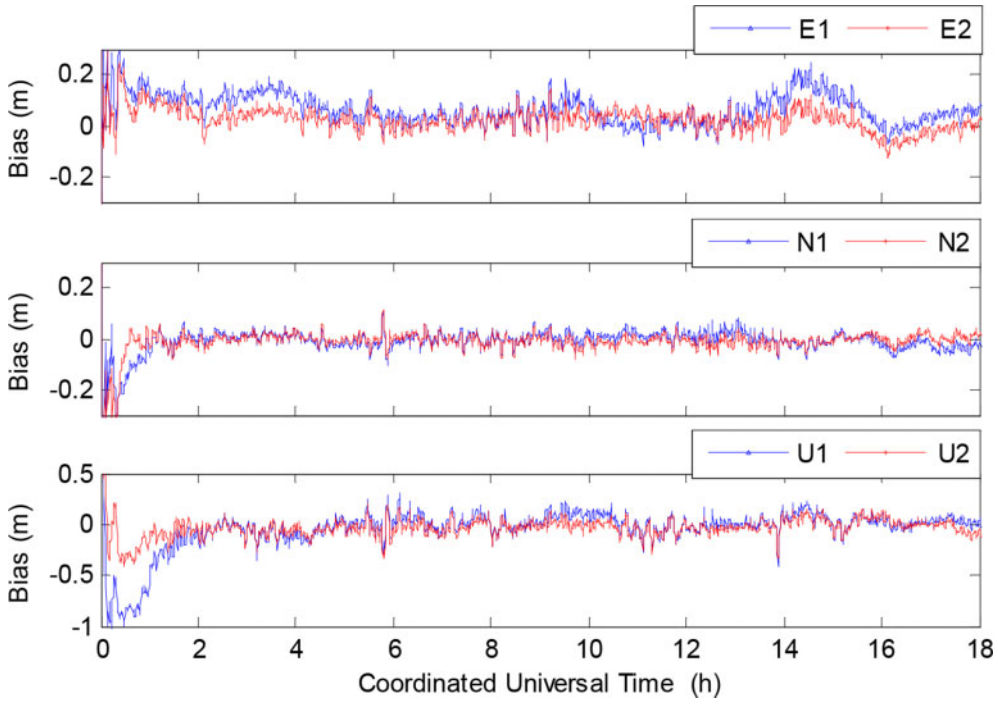

8 Positioning bias at NKLG in the East (E), north (N), and upward (U) directions using the two schemes described here

the whole period. This is reasonable because the prior stochastic model in Scheme 1 may be inappropriate because it overestimates the errors for the ionosphere-free combined observations. In Scheme 2, the adaptive pseudo-range noise estimation method was used to track the time-varying characteristics of pseudo-range noise at different frequencies in real time. Consequently, the stochastic characteristics of observation noise can be described more accurately. As a result, more reasonable prior variances can be used for PPP, so that positioning accuracy and convergence speed can be greatly improved.

Similarly, Fig. 9 shows the positioning results for the ALIC station using the two schemes during UTC 9:00–15:00. Figure 10 shows the elevation angle variation for all satellites. The dotted blue line reflects the elevation variation of Satellite G01; the other satellites are not distinguished. It is worth mentioning that only a specific period rather than the whole session of solutions are given in Figs. 9 and 10 for the sake of convenience. Therefore, no convergence procedure can be observed in Fig. 9.

As shown in Fig. 9, the positioning performance of Scheme 2 was more accurate than that of Scheme 1, especially when the elevation of satellite G01 was

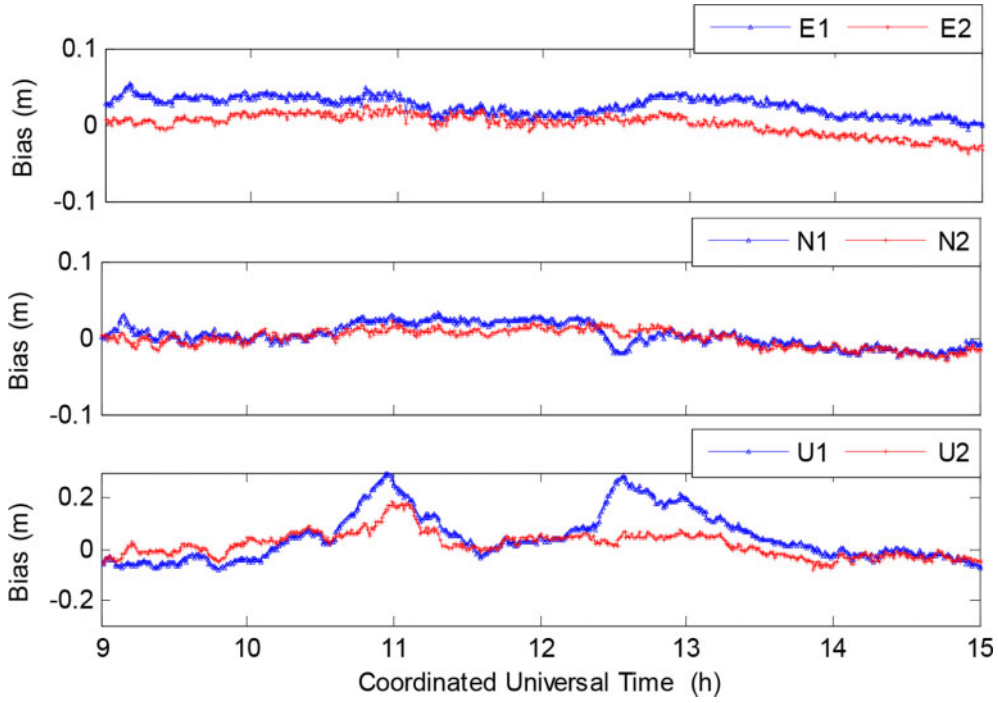

9 Positioning bias at ALIC using the two schemes

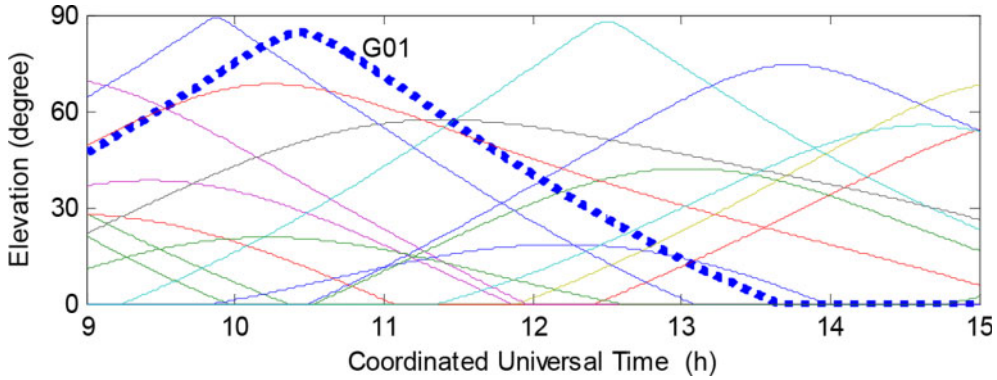

10 Variation of satellite elevation at ALIC

high enough. This is reasonable considering that the abnormal G01 satellite data decreased the positioning accuracy of Scheme 1, particularly when the satellite rose to a high elevation angle. More importantly, the elevation angle of satellite G01 was higher than that of any other satellite during UTC 10:30–11:30, as shown in Fig. 10. Therefore, when Scheme 1 was used to develop the stochastic model, satellite G01 with the abnormality was assigned the smallest variance. In other words, satellite G01 played a greater role than the other satellites in positioning. During UTC 12:00–13:00, although the elevation angle of satellite G01 was not the highest, the position accuracy loss caused by the observation abnormality was still serious. From the perspective of external reliability, if this kind of abnormality has not been correctly detected, it will decrease the ability of the positioning system to overcome possible model errors and will influence the precision of parameter estimates.

In addition to the abnormal data, datasets retrieved from ~20 globally distributed IGS stations were processed using the above two schemes. Results show that most solutions of the two different schemes agree well with each other. In other words, the proposed method also applies to the normal GPS data without sacrificing the positioning accuracy. This is reasonable when we acknowledge the following two facts: on the one hand, the quality of most IGS data is good and thus the positioning accuracy will not be seriously degraded; on the other hand, the final estimates mainly depend on the carrier-phase observations if the pseudo-ranges are not polluted. For the sake of simplicity, the positioning results are not presented herein since no significant improvement can be observed.

Conclusions

In this paper, the stochastic characteristics of GPS pseudo-range noise have been analysed, demonstrating that the noise level of GPS observations is significantly affected by various factors. Hence, it is not appropriate to use a single empirical model to describe GPS observation errors under all observing conditions. An adaptive stochastic model, which estimates pseudo-range noise with sliding windows, has been developed to construct a more appropriate stochastic model. Experimental results showed that compared to the traditional stochastic model, the new method can describe the stochastic characteristics of GPS observation noise more accurately. Therefore, this method can significantly improve positioning accuracy and convergence performance.

Acknowledgements

The authors gratefully acknowledge IGS for providing GNSS data and products. Authors also appreciate the editor-in-chief, Peter Collier, and two anonymous reviewers for their valuable comments and improvements to this manuscript.

References

De Bakker, P. F., Tiberius, C. C. J. M., van der Marel, H. and van Bree, R. J. P. 2012. Short and zero baseline analysis of GPS L1 C/A, L5Q, GIOVE E1B, and E5aQ signals. *GPS Solutions*, 16(1), pp.53–64.

De Bakker, P. F., van der Marel, H. and Tiberius, C. C. J. M. 2009. Geometry-free undifferenced, single and double differenced analysis of single-frequency GPS, EGNOS, and GIOVE-A/B measurements. *GPS Solutions*, 13(4), pp.305–14.

Dow, J. M., Neilan, R. E. and Rizos, C. 2009. The International GNSS service in a changing landscape of global navigation satellite systems. *Journal of Geodesy*, 83(7), pp.191–8.

Estey, L. and Meertens, C. 1999. TEQC: the multi-purpose toolkit for GPS/GLONASS data. *GPS Solutions*, 3(1), pp.42–9.

He, H. 2002. *GPS dynamic measurement and quality control in high accuracy*. PhD thesis. The PLA Information Engineering University.

IGSSTATION-3728. 2010. ALIC: ME upgrade: IGS Mail., Available at: <http://igscb.jpl.nasa.gov/mail/igsstation/2010/msg00252.html>.

IGSSTATION-3860. 2010. ALGO communications down: IGS Mail., Available at: <http://igscb.jpl.nasa.gov/pipermail/igsstation/2010/002972.html> p.0.

Kouba, J. and Héroux, P. 2001. Precise point positioning using IGS orbit and clock products. *GPS Solutions*, 5(2), pp.12–28.

Satirapod, C. and Luansang, M. 2008. Comparing stochastic models used in GPS precise point positioning. *Survey Review*, 40(308), pp.188–94.

Tiberius, C. and Kenselaar, F. 2000. Estimation of the stochastic model for GPS code and phase observables. *Survey Review*, 35(277), pp.441–54.

Wang, J., Satirapod, C. and Rizos, C. 2002. Stochastic assessment of GPS carrier phase measurements for precise static relative positioning. *Journal of Geodesy*, 76(2), pp.95–104.